Multiple phase transitions found in a magnetic Heusler alloy and thermodynamics of their magnetic internal energy

Jason N. Armstrong, James D. Felske, and Harsh Deep Chopra*
Laboratory for Quantum Devices, Materials Program, Mechanical and Aerospace Engineering Department, State University of New York at Buffalo, Buffalo, New York 14260, USA
(Received 6 January 2010; revised manuscript received 8 March 2010; published 7 May 2010)

The Ni-Mn-Ga Heusler alloy is one of the most widely investigated multiferroic material. While this system is well known to undergo a martensitic phase transformation as well as premartensitic transitions and anomalies, the present study reports the observation of multiple phase transitions occurring over a narrow temperature interval (including three lock-step martensitic transformations) whose detection, corroboration, and visualization is made through the use of several complementary techniques and methods. The spontaneous magnetization of various phases and their temperature dependence is experimentally derived, which provides fundamental information related to electrons contributing to the observed magnetism for each phase. The dynamics of micromagnetic reconfiguration across phase transitions show the remarkable feature of a system with an infinite number of available pathways resembling a devil's staircase as it repeatedly achieves the same final magnetic state. Using experimental values of specific magnetization, the field and temperature dependence of molecular-field coefficient is estimated. From thermodynamics considerations it is shown that as a general rule, the magnetic specific heat can be taken as equal to the difference in heat capacities at constant field and magnetization, and its field and temperature dependence is experimentally deduced. Finally, the form of the function for intrinsic specific magnetization is formally derived, which was previously cited by Stoner [Philos. Mag. **19**, 565 (1935)] by inspection alone.

DOI: 10.1103/PhysRevB.81.174405 PACS number(s): 75.30.Cr, 75.85.+t, 75.60.Ej

I. INTRODUCTION

A common feature underlying the adaptive behavior of most functional materials is a structural phase transformation that results in the formation of ferroelastic domains in the low temperature, lower symmetry product phase. Prototypical examples include formation of ferroelastic domains following paraelectric to ferroelectric Curie transition in barium titanate,[1–3] paramagnetic to antiferromagnetic Néel transition in NiO,[4,5] martensitic phase transition in shape memory alloys,[6] etc. The "ferroelastic" domain walls can be displaced by both the operative "ferroic" force field characteristic of the material (electric, magnetic, etc.) as well as by mechanical load. Naturally, the physical properties and technological applications of ferroic materials depend, to a considerable extent, on the characteristics (such as thermoelasticity, thermal hysteresis, etc.) of phase transformation(s) that leads to the formation of ferroelastic domains; see, for example, Refs. 7–10 for controlled synthesis of hierarchical polydomain structures in shape memory alloys and their mechanical properties. Shape memory alloys are particularly illustrative of this concept, where the chemical free energy for transformation is balanced by elastic strain energy, which essentially creates equivalence between temperature (thermally induced transformation) and stress (stress-induced transformation). With the advent of magnetic shape memory alloys,[11,12] the magnetic energy also has to be factored in the overall driving force for the phase transformation.[13–33]

The Ni-Mn-Ga Heusler alloy is one of the most widely investigated magnetic shape memory alloy. This system is well known to undergo a martensitic transformation[34] as well as premartensitic transitions and anomalies in its physical properties.[35–42] Remarkably, the present study reports the observation of multiple phase transitions in this system over a narrow temperature interval using several complementary techniques and methods. The dynamics of micromagnetic reorganization, and therefore by default, the formation of ferroelastic domains that host the micromagnetic domains, resembles a devil's staircase.[43–54] Results are followed by a treatise on thermodynamics of magnetic phases, derivation of spontaneous magnetization for each phase as well as their field and temperature dependence, and estimation of molecular-field coefficient as a function of temperature and magnetic field. Thermodynamic considerations show that the magnetic specific heat (excess specific heat in a ferromagnet compared to a similar material devoid of ferromagnetism) is equal to the difference in heat capacities at constant field and magnetization. Finally, the form of the function for intrinsic specific magnetization is formally derived.

II. EXPERIMENTAL DETAILS

The single-crystal Ni-Mn-Ga alloy in the present study had a nominal composition of $Ni_{52}Mn_{23}Ga_{25}$ corresponding to e/a ratio of 7.56. This alloy composition was previously investigated in relation to the effect of e/a ratio on phonon softening by Mañosa *et al.*,[42] from whom the sample was obtained. The ac susceptibility measurements and dc magnetic measurements were made in a 7 T Quantum Design physical property measurement system. The optical observations of the microstructure as a function of temperature were made by placing the sample in a commercially available precision heating and cooling stage (Linkam, England) having an accuracy of ± 0.1 °C, as described in detail in a previous publication.[19] The fully automated stage acquires and labels all images during preprogramed heating/cooling cycles to en-

sure unambiguous correlation between the microstructure as a function of temperature. While heating and cooling curves were measured for dc magnetization, ac susceptibility, and magnetic transition spectra, for clarity, cooling, and heating curves are only shown for ac susceptibility since it is the tool of choice for detecting phase transitions. Other data show similar thermal hysteretic behavior for cooling versus heating.

The dynamical measurements of micromagnetic reconfiguration as a function of temperature accompanying phase transitions were made using the method of magnetic transition spectrum (MTS), which is described in detail elsewhere[20,55] and briefly summarized in the following for convenience. The MTS method is an electronic method that can monitor dynamical changes in the micromagnetic structure as a function of temperature, stress, or any other force field. It is based on the same principle upon which the well-known Barkhausen method is based,[56] namely, Faraday's law: voltage ξ, induced in a pickup coil is proportional to the rate of change in flux with time $\xi=-d\Phi/dt$ in a sample, where $d\Phi$ is the flux change over a time interval dt. Whereas the conventional Barkhausen method generates a spectrum of voltage spikes by placing a pickup coil next to a ferromagnetic sample and cycling the sample in an applied magnetic field, the MTS method generates a spectrum of voltage spikes by sweeping the sample across the transformation temperature, load, or any other force field.[20,55,57] The experimental setup used in the MTS method is similar to that for the Barkhausen method.[58,59] However, instead of an energizing field coil to sweep the sample across the hysteresis loop, for temperature-dependent MTS, a heating/cooling stage is used to sweep the sample across the phase transition(s) (the schematic is later shown in the inset of Fig. 11). The signal pickup coil is fabricated out of an insulating ferrite core, whose output is typically bandwidth limited by a band pass filter to a range of 1–10 kHz. The pickup coil is a miniature probe in the form of a hemispherical ring 2–3 mm in diameter, 1 mm thick and having 50–100 encircling coil turns. The sample is attached to the probe and placed in a commercial temperature stage (Linkam, England) that is capable of heating and cooling the sample from 77 to 873 K to within ± 0.1 K while allowing simultaneous observation of the structural changes in an optical microscope. The stage is fully automated and interfaced with an image frame grabber (Linkam) and a high-speed data-acquisition card. Furthermore, the experimental setup acquires and labels all images and data automatically following the execution of a preprogramed heating/cooling cycle. The experimental information (temperature, heating/cooling rate, etc.) is automatically collated and numbered by the software. This degree of automation ensures unambiguous correlation between the microstructure and the acquired MTS spectrum as a function of temperature.

III. RESULTS AND DISCUSSION

A. Martensitic and premartensitic phase transitions

When the Ni-Mn-Ga single crystal is cooled below its martensite transformation temperature, the austenite phase spontaneously breaks up into ferroelastic domains in the form of crystallographic twins; see, for example, the optical micrograph of the fully transformed martensite in this crystal at 189.1 K in Fig. 1. It is important to recognize that in addition to the structural transformation, the alloy also simultaneously undergoes a magnetic phase transition on account of change in electronic structure from austenite to the martensite phase. This leads to a change in both the magnitude and orientation of magnetocrystalline anisotropy axes. As a result, the magnetocrystalline anisotropy axes in the martensite phase gets reoriented and redistributed over length scales on the order of twin width. Therefore the resulting martensite phase not only has a high density of twins (structural heterogeneity) but each twin also hosts a multiplicity of magnetic domains; see Refs. 18, 19, 28, and 57 for detailed studies on the temperature-dependent micromagnetic structure in Heusler alloys. Consequently, there is an *apparent* drop in the measured magnetic moment when the applied bias fields is insufficient to achieve saturation magnetization (found to be ≤ 10 kOe in the present study), as shown in Fig. 2. The key point being that there is no fundamental meaning to the magnitude of this drop because it arbitrarily depends on the size, scale, and distribution of twins hosting the magnetic domains. Figure 2 shows that only when the bias field exceeds ~ 10 kOe, the measured magnetization becomes equal to the intrinsic specific magnetization $\sigma_{H,T}$ at the given temperature and field. Below this field strength, the magnetization processes are mainly hysteretic and thermodynamic treatment discussed later does not apply. From Fig. 2, also note that whereas saturation of the martensite phase require fields in excess of ~ 10 kOe, the parent phase achieves saturation magnetization at fields in excess of only ~ 5 kOe; lack of saturation in the austenite phase at lower fields is evident from the near zero slope of the $\sigma_{H,T}$ versus T in Fig. 2. These observations were also separately confirmed by the measurement of hysteresis loops at different temperatures, which is discussed below in relation to the derivation of the spontaneous magnetization $\sigma_{0,T}$ as a function of temperature. The inset in Fig. 2 shows a zoom-in view of specific magnetiza-

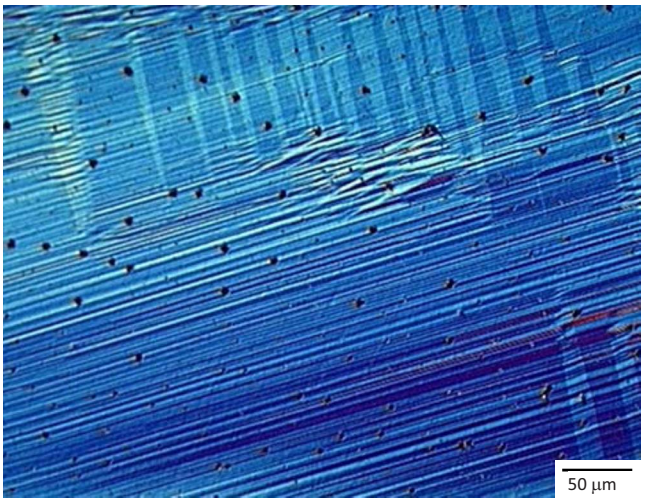

FIG. 1. (Color online) Diagonal and vertical bands of interpenetrating martensite twins in Ni-Mn-Ga at 189.1 K, which is below the martensite finish M_f temperature.

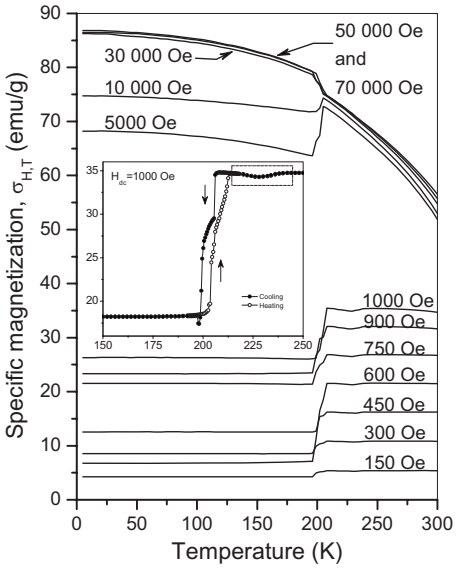

FIG. 2. (a) Temperature dependence of specific magnetization at different dc bias field in Ni-Mn-Ga alloy during cooling. The inset shows a zoom-in view of the premartensitic and martensitic transitions for both cooling and heating cycles at a dc bias field of 1 kOe, indicating the existence of multiple phase transitions and highlighting thermal hysteresis associated with phase transitions in cooling versus heating.

tion versus temperature curves for both cooling and heating cycles at a bias field of 1 kOe. Notice the existence of two distinct steps during the martensitic transition during both cooling and heating. Also, note the section of the curve enclosed within the dotted box, which is indicative of additional phase transitions above the martensite transition and evident from the presence of two inflection points $[(\partial^2\sigma/\partial T^2)_H=0]$.

In contrast to dc measurements, the dynamic or ac susceptibility method is a sensitive and a better suited probe for detecting magnetic phase transitions. Additionally, when ac susceptibility measurements are made at different dc bias fields, the resulting field dependence of differential susceptibility can provide further insight into the nature of competing magnetic interactions. As shown in Fig. 3(a), ac susceptibility of the sample clearly reveals the existence of multiple phase transitions, where the real component (χ') of ac susceptibility is plotted for both cooling and heating (although shown truncated for clarity, the measurements were made down to 2 K). In Fig. 3(a), vertical arrows indicate critical points of various phase transitions; the determination of Curie temperature Θ_c is discussed later. In the following, in addition to ac susceptibility, the existence of these transitions was independently corroborated by a number of complementary methods, including (a) the derivation of the fundamental property of any magnetic phase, namely, spontaneous magnetization, as a function of temperature, which shows clear jumps in atomic magnetic moment at the marked transition points, (b) direct optical observation of structural changes associated with several of these phase transitions, and (c) measurement of magnetic transition spectrum.

First consider the temperature interval where the martensitic phase transition occurs. In sharp contrast to dc measure-

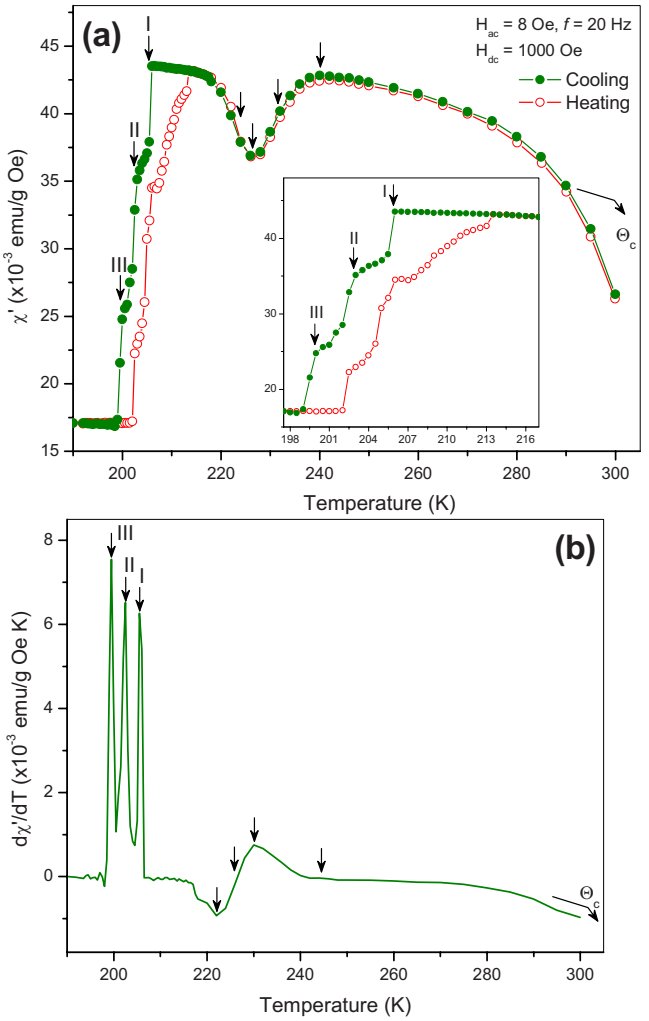

FIG. 3. (Color online) (a) The real component of ac susceptibility of the Ni-Mn-Ga alloy as a function of temperature for both cooling and heating. Vertical arrows indicate multiple phase transitions. The inset shows the zoom-in view of the three successive martensitic transitions (labeled I, II, and III) for both cooling and heating cycles and highlight the associated thermal hysteresis for cooling versus heating. (b) The derivative of real component of susceptibility for cooling cycle, which shows three distinct peaks associated with the three martensitic transitions as well as critical points for other premartensitic transitions.

ments in Fig. 2, ac magnetic susceptibility of the sample clearly reveals the existence of three distinct martensitic phase transitions, labeled I, II, and III in Fig. 3(a). For clarity, the inset in Fig. 3(a) shows the zoom-in view of the temperature interval where the three martensitic transitions occur. These three distinct transitions can also be seen clearly in the $d\chi'/dT$ versus T plot in Fig. 3(b) corresponding to the cooling cycle in Fig. 3(a). The existence of multiple martensitic phase transitions was directly corroborated by temperature-dependent optical microscopy using Nomarski polarization interferometer optics, which is sensitive to nanometer scale changes in surface unevenness due to structural changes. The attached movie clearly shows the three consecutive "austenite-martensite" interfaces sweeping the same volume of the sample as the sample is being cooled.[60] From

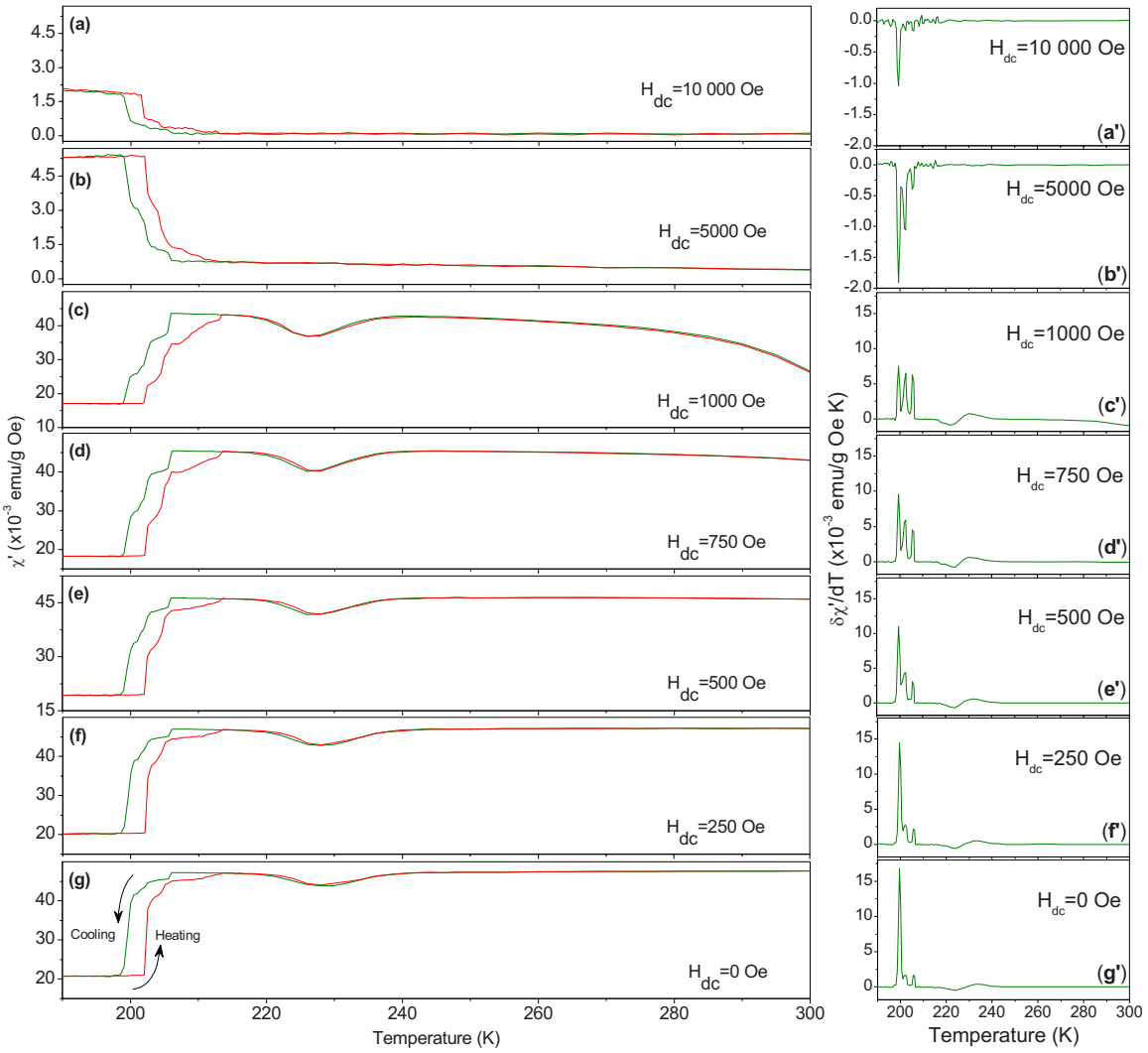

FIG. 4. (Color online) [(a)–(g)] χ' versus temperature curves for both cooling and heating at different dc bias fields. [(a′)–(g′)] $d\chi'/dT$ versus temperature curves corresponding to the cooling cycles in (a)–(g), respectively.

the movie, the fact that these transitions sweep across the same volume of the sample eliminates possible spurious effects arising from composition gradients. As shown in the following, each of these transformations is further confirmed by the observed jumps in *intrinsic spontaneous magnetization* of the crystal, which completely eliminates any spurious possibility arising from size, shape, structure, or any other defect related disorder. An interesting feature of these consecutive martensitic phase transitions is that once the austenite (parent phase) transforms into martensite-I, then for the next martensitic transition, martensite-I serves as the "austenite" phase that transforms into martensite-II, and similarly, martensite-II serves as the austenite phase that transforms into martensite-III. However, occurrence of multiple martensite transformations is not uncommon. It is well known to occur even in single elements such as plutonium, and is related to intrinsic commensurate/incommensurate structural modulations that trigger successive martensitic transformations.[61] Determination of the precise role of structural modulations in the present alloy is beyond the scope of the present study.

The ac susceptibility was further measured at different dc bias fields. Figures 4(a)–4(g) shows real component (χ') of ac susceptibility for both cooling and heating cycles at dc bias fields ranging from zero [Fig. 4(g)] to 1 T [Fig. 4(a)]. Figures 4(a′)–4(g′) are the corresponding $d\chi'/dT$ versus T cooling curves corresponding to Figs. 4(a)–4(g), respectively. Figure 4 shows that the three successive martensitic phase transitions become progressively more pronounced and well delineated as the dc bias field approaches ~750–1000 Oe. Moreover, the fact that three separate peaks are still (although barely) discernible even at zero field in Fig. 4(g′) is what enabled the optical visualization of these three transitions in the attached movie.

Figures 3 and 4 also reveal the existence of several (weak) premartensitic phase transitions. In fact, their existence in the present study was found during temperature-dependent optical microscopy using Nomarski polarization interferometer optics. Beginning with a sudden change in optical contrast near ~230–240 K [near the beginning of the premartensite dip in χ' in Fig. 3(a)], Nomarski interferometer images revealed the gradual emergence of a striated pattern that in-

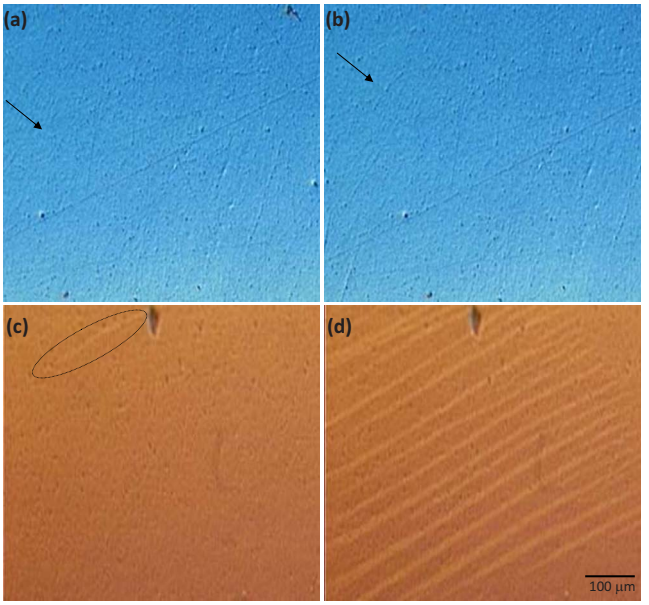

FIG. 5. (Color online) [(a)–(d)] Gradual emergence of twinlike premartensitic structure at different temperatures during cooling. (a) 219.9 K, (b) 218.8, (c) 217 K, and (d) 216.2 K. Micrographs (a) and (b) were taken at a different region compared to (c) and (d).

creased in contrast upon cooling. Figures 5(a) and 5(b) shows, respectively, the observed striated pattern at two different intermediate temperatures (at higher temperatures the striated pattern is visible but becomes too faint to be clearly shown here. The arrows in Figs. 5(a) and 5(b) indicate that the striations run diagonally from top-left to bottom-right. In terms of Nomarski interferometery, the gradual increase in surface relief implies that the strain associated with premartensitic transitions, although very small, increases with a decrease in temperature. While time-dependent studies are beyond the scope of the present study, the striated pattern depended on cooling rate, with faster cooling rates delaying or entirely suppressing the formation of the premartensitic structure. These observations point to thermal (diffusion-based) nature of the premartensitic transitions, as opposed to the athermal or diffusionless nature of the aforesaid martensitic transitions. Figures 5(c) and 5(d) show another subsequent phase transition in another portion of the sample that becomes visible at ~218 K (labeled as δ-ω transition in Fig. 10 later). In Fig. 5(c), the dotted line encircles the first surface relief associated with this phase transition that became visible in the field of view of the microscope.

Figure 4 also shows that in comparison to the martensitic transitions, the ac susceptibility of premartensitic transitions is a relatively weak function of temperature. Moreover, field dependence of differential susceptibility in the premartensitic regime was found to vary sharply with dc bias field. Therefore to study the evolution of the premartensitic "dip" in χ', measurements were made at small increments of dc bias field. Figure 6 plots a subset of dc bias fields at which ac susceptibility was measured, which shows that the premartensitic phase transitions begin to be resolved as the dc bias field increases to ~1100–1400 Oe. A further subset of these curves is shown in the zoom-in view in Fig. 7, which

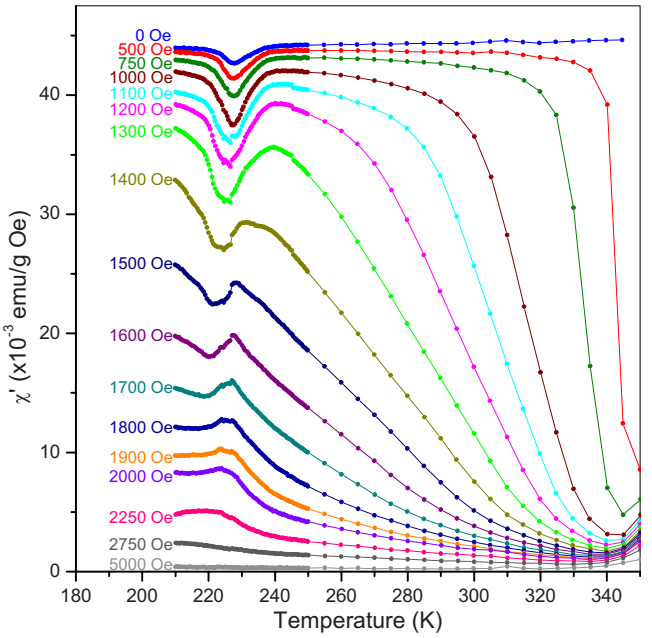

FIG. 6. (Color online) [(a)–(g)] χ' versus temperature curves for cooling at different dc bias fields to study the field dependence of premartensitic transitions. Since there is minimal thermal hysteresis in cooling versus heating for transitions occurring in the premartensitic regime, only cooling cycles are shown.

shows more clearly the evolution of various critical points (except for the marked β-γ transition that was harder to resolve). As shown in the next section, these phase transitions corroborate well with jumps in intrinsic spontaneous magnetization versus temperature. Figure 6 also shows that the premartensitic anomalies disappear at fields in excess of ~2700 Oe. The micrographs in Fig. 5 clearly show that the premartensitic transitions are accompanied by successive lattice distortions. Recently, Ludwig *et al.*[62] have conducted

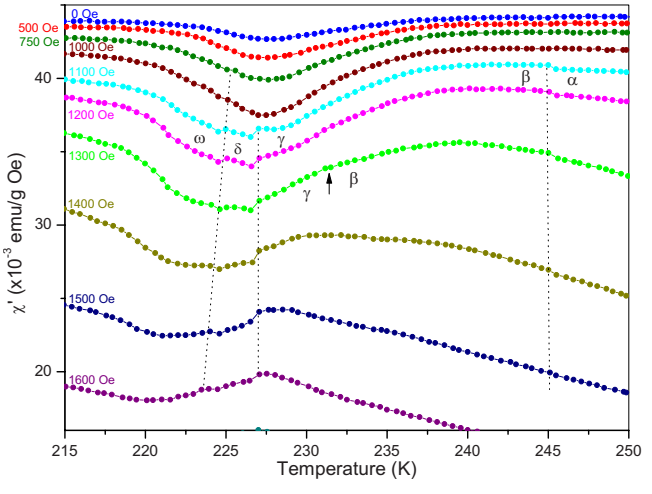

FIG. 7. (Color online) [(a)–(g)] A zoom-in view of a subset of χ' versus temperature curves for cooling at different dc bias fields to study the evolution of various critical points in the premartensitic regime. Since there is minimal thermal hysteresis in cooling versus heating for transitions occurring in the premartensitic regime, only cooling cycles are shown.

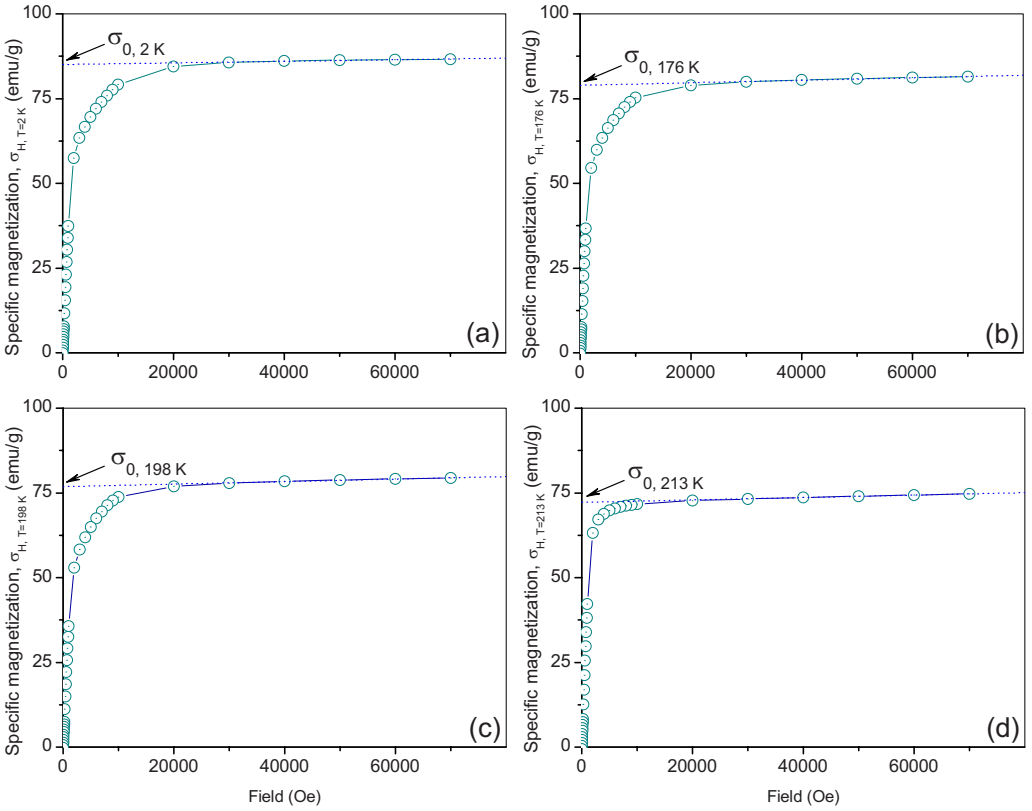

FIG. 8. (Color online) [(a)–(d)] Four illustrative examples of measurement of spontaneous magnetization at four different temperatures using the magnetic isotherm method. Prior to each measurement, the sample was demagnetized. Measurements are shown for cooling cycle.

acoustic emission studies of the premartensitic transitions using a crystal that was cut from the same boule used in the present study. Their studies revealed that the premartensitic acoustic emissions vanished at fields in excess of ~2.5 kOe, in agreement with results shown in Fig. 6. The disappearance of premartensitic anomalies in ac susceptibility measurements may then be directly linked to the ability of the applied field to suppress the formation of multiple ferroelastic domains of the type shown in Fig. 5. Combined with a small difference in intrinsic spontaneous magnetization between successive phases (as shown in the next section), energetically, the crystal transitions from a single domain (ferromagnetic as well as ferroelastic) of one phase into a single domain of the successive phase.

Derivation of spontaneous magnetization $\sigma_{o,T}$

The fundamental quantity of interest in characterizing any given magnetic phase is its spontaneous magnetization $\sigma_{o,T}$ —*magnetization within a single magnetic domain of the crystal at zero magnetic field*—and its variation with temperature. It is an intrinsic property of a magnetic material, independent of the size, shape, or technique used to determine it. This quantity is also of interest in the theory of ferromagnetism as it provides fundamental information related to electrons contributing to the observed magnetism and in formulating the law of states, viz., ratio of spontaneous magnetization to spontaneous magnetization at absolute zero temperature $\sigma_{o,T}/\sigma_{o,o}$ versus the reduced temperature T/Θ_c. With the aforesaid observation of a large number of phases, it therefore becomes necessary to determine the spontaneous magnetization of various phases as a function of temperature.

Practically, the measurement of spontaneous magnetization is complicated by the fact that a magnetic material generally exists as an aggregate of magnetic domains and a direct measurement of spontaneous measurement within a single domain is not possible. While application of magnetic fields can erase magnetic domains, *the resulting quantity is not spontaneous magnetization* $\sigma_{o,T}$ but rather intrinsic magnetization at a finite field $\sigma_{H,T}$. To overcome this problem, three principal extrapolation and interpolation methods were originally developed by Weiss and Forrer,[63] and Sucksmith and co-workers.[64] Two of these methods (used in the present study) involve measurement of magnetization as a function of field at different temperatures (the so-called magnetic isotherm method and the method of curves of constant magnetization) while the third is based on measurement of the magnetocaloric effect.

Briefly, to determine spontaneous magnetization $\sigma_{o,T}$ at a given temperature, the magnetic isotherm method involves the measurement of magnetization as a function of applied field at a given temperature, followed by extrapolation of the linear, high-field portion of the curve to zero field. Measurements are made at various temperatures and examples of spontaneous magnetization obtained by this method at four different temperatures are shown in Figs. 8(a)–8(d). Note that the magnetic isotherm method is less reliable at temperatures in the vicinity of the Curie temperature, where the slope

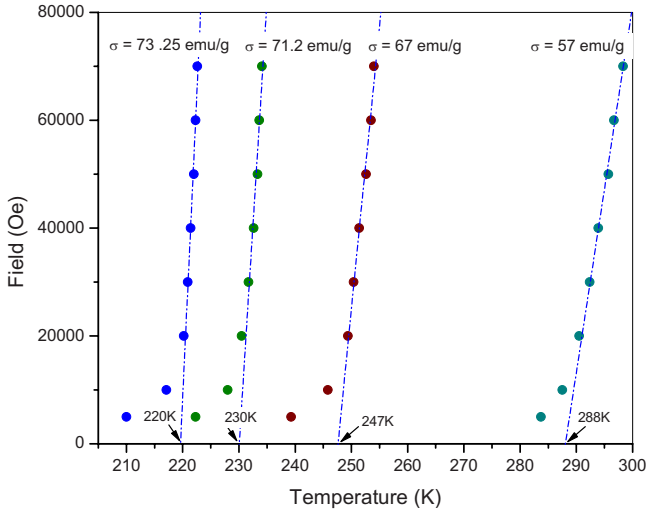

FIG. 9. (Color online) [(a)–(d)] Illustrative examples of measurement of spontaneous magnetization using the method of constant magnetization. Measurements are shown for data acquired for cooling cycle.

of the high-field portion of the magnetization may not be close to zero or may become nonlinear. Hence the use of different methods for determination of $\sigma_{o,T}$.

The method of constant magnetization measures magnetization as a function of temperature at different static fields, followed by interpolation of data to obtain a series of magnetic field (ordinate) versus temperature (abscissa) curves at fixed values of magnetization. At high fields and sufficiently high values of magnetization, the linear portions of such field versus temperature curves can be extrapolated to zero field and the point on the abscissa where the curve of constant magnetization intersects gives the temperature corresponding to the spontaneous magnetization for the given value of magnetization, as shown in Fig. 9. This method is applicable at low as well as temperatures approaching the Curie temperature.

Using these two methods, the variation in spontaneous magnetization versus temperature is shown in Fig. 10(a). It shows a series of jumps in spontaneous magnetization for the alloy. *Note that spontaneous magnetization measures electrons contributing to the observed magnetism and is an intrinsic property of a material. Therefore, jumps in spontaneous magnetization are the unambiguous indications of magnetic phase transitions*, as indicated by the vertical arrows in Fig. 10(a). The inset in Fig. 10 shows a plot of square of spontaneous magnetization $\sigma_{o,T}^2$ versus temperature, which when extrapolated linearly to the abscissa gives a value of ~389 K for the Curie point. This value is consistent with previous determination of Curie temperature in this alloy using thermal analysis.[42] Figure 10(b) plots the derivative of the square of spontaneous magnetization versus temperature. In the following thermodynamics treatment, it will be shown that $(-1/2)(\partial\sigma^2/\partial T)_H$ at a given field (including zero field corresponding to spontaneous magnetization) is proportional to the ratio of excess specific heat due to magnetization C_M to $(N\rho)$, where $(N\rho)$ is the coefficient of molecular field $H_m=(N\rho)\sigma$ and ρ is the density. [Note that when

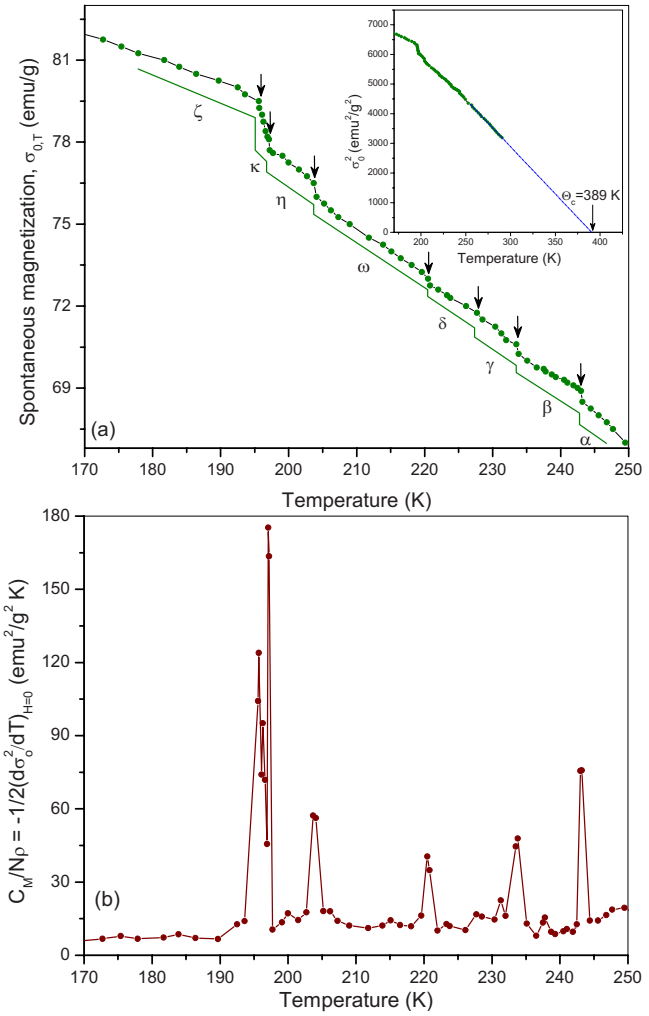

FIG. 10. (Color online) (a) Variation in spontaneous magnetization versus temperature of the Ni-Mn-Ga alloy during cooling. Inset shows the square of the spontaneous magnetization versus temperature, whose extrapolation to abscissa gives the Curie temperature. (b) Derivative of square of spontaneous magnetization versus temperature for cooling.

expressed in terms of moment per unit volume M instead of specific magnetization (per unit mass), the molecular-field coefficient becomes equal to N instead of $N\rho$ such that $H_m=NM=N\rho(M/\rho)=(N\rho)\sigma$].

Associated with the observed phase transitions are a catastrophic or avalanchelike reconfiguration of the magnetic structure as the crystal transforms from one phase to another. This gives rise to a magnetic transition spectrum of voltage spikes reflecting the dynamics of the magnetic transitions. It also provides yet another means of following the progression of these various phase transitions. Figure 11 shows the acquired magnetic transition spectrum on cooling. The inset in Fig. 11 is a magnified view of the acquired spectrum in the premartensitic regime along with a schematic of the experimental setup used to acquire the spectrum. Figure 11 clearly shows the avalanchelike distributions of the induced pulses across the temperature interval where various phase transitions occur. Previously, the authors have used a "jumpsum" method to analyze and interpret magnetic transition spectra

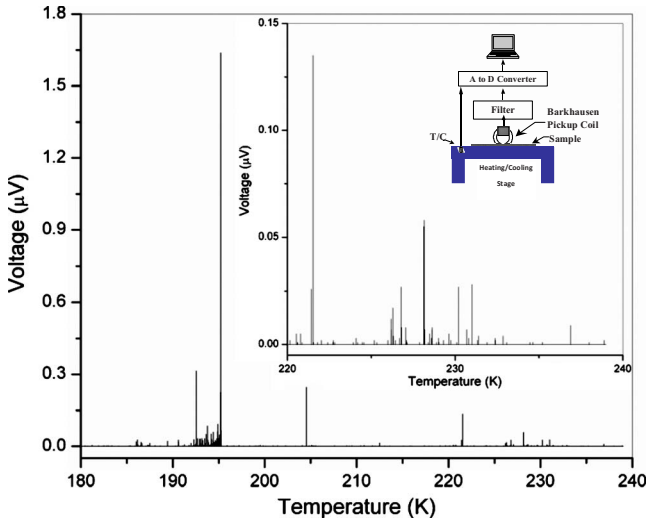

FIG. 11. (Color online) Magnetic transition spectrum of Ni-Mn-Ga on cooling. Inset shows a zoom-in view of the spectrum in the premartensitic regime. The schematic shows the experimental setup used for acquiring the spectrum (T/C: thermocouple).

such as the one shown in Fig. 11.[20,55] Instead of assigning an average value for the entire spectrum, the jumpsum *JS* analysis expresses the acquired signal in terms of the profile of the spectrum and *JS* is simply the running total of all the voltage spikes, as shown in Fig. 12. The *i*th value of *JS* is equal to the sum of all preceding voltage jumps $\Sigma_{i=1}^{i}\xi_i$. up to that temperature (from right to left on cooling in Fig. 12). The lower portion of Fig. 12 shows the *JS* curve for the spectrum shown in Fig. 11. The inset shows the magnified view of the β-γ portion of the *JS* curve. To illustrate various transition temperatures, Fig. 12 also overlay the plot of spontaneous magnetization versus temperature shown earlier in Fig. 10(a). It is also important to make a distinction between the

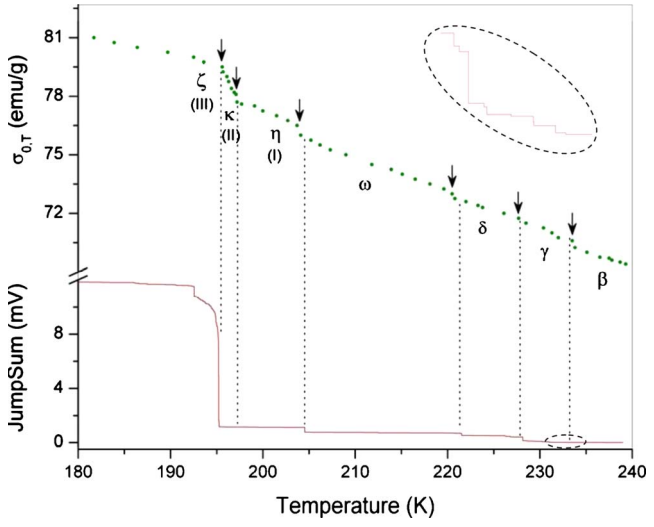

FIG. 12. (Color online) Jumpsum (lower curve) of the magnetic transition spectrum for the Ni-Mn-Ga sample on cooling. The curve of spontaneous magnetization versus temperature (upper curve) during cooling is also shown above the Jumpsum curve. Inset shows the zoom-in view of the β-γ portion of the Jumpsum curve.

meaning of a large number of voltage spikes in the spectrum shown in Fig. 11 versus a single discontinuity associated with an observed physical property (such as ac susceptibility, Figs. 3 and 4, or spontaneous magnetization, Fig. 10) at each transition temperature. Multiple voltage spikes in the spectrum are due to reconfiguration of magnetization vectors in a multitude of tiny magnetic domains in the crystal. In other words, each voltage spike is not a phase transition but reflects the individual dynamics of many domains as the system undergo a phase transition.

Using the MTS method, the dynamics of any phase transition can be further explored by repeatedly cycling the sample across a given temperature interval. This is shown in Fig. 13 for the case of transition from a fully transformed martensite(III) to martensite(III-II) phase region. Figure 13(a) shows minor dc magnetization loops over successive cycling between 195 and 201.8 K. For ease, the ac susceptibility loop for cooling and heating (shown earlier in Fig. 3) is also replotted in the inset of Fig. 13(a) in order to highlight the portion of the overall transition region across which the temperature excursion was made (marked schematically in the encircled region). Figure 13(b) shows the successive JS curves during both cooling (1C-4C) and heating (1H-3H). The remarkable feature of the *JS* curves (either for cooling or for heating) is that the saturation value of *JS* is the same even though the actual transition pathways leading to the saturation *JS* value is different for each cycle, as shown in the zoom-in view for the three successive *JS* curves for cooling in Figs. 13(c)–13(e). This observed dynamics of underlying micromagnetic reconfiguration reveals the remarkable feature of a system having an infinite number of available pathways resembling a devil's staircase as it repeatedly achieves the same final magnetic state. Note that the magnetic domains are superimposed on the ferroelastic domains. Therefore by default, the formation of ferroelastic domains also resembles a devil's staircase. The actual formation and annihilation of ferroelastic domains during repeated heating and cooling, corresponding to the *JS* curves shown in Fig. 13, was recorded and is shown in the second movie attached along with this submission.[60] This movie shows that while the process of repeated annihilation and reformation of ferroelastic domains is nearly the same, there are always small differences in the process. These differences, however small, causes the system to take a new pathway each time, which is reflected in the observed *JS* curves. The reason for a different saturation value of *JS* for cooling versus heating is described in a previous publication.[20]

B. Thermodynamics of magnetization

Next consider the form of the thermodynamic function for the dependence of internal energy on specific magnetization, viz., $(\partial E/\partial\sigma)_T$. From such an expression, various σ-dependent thermodynamic properties can be derived and molecular-field coefficient $N\rho(T,H)$ modeled. Later, the form of the function $\sigma(H,T)=f(\eta)$ will be formally derived, which Stoner had earlier cited by inspection alone from the expression for $(\partial E/\partial\sigma)_T$.[65] In addition, the applicability and caveats for use of the following equations for a single phase will be discussed.

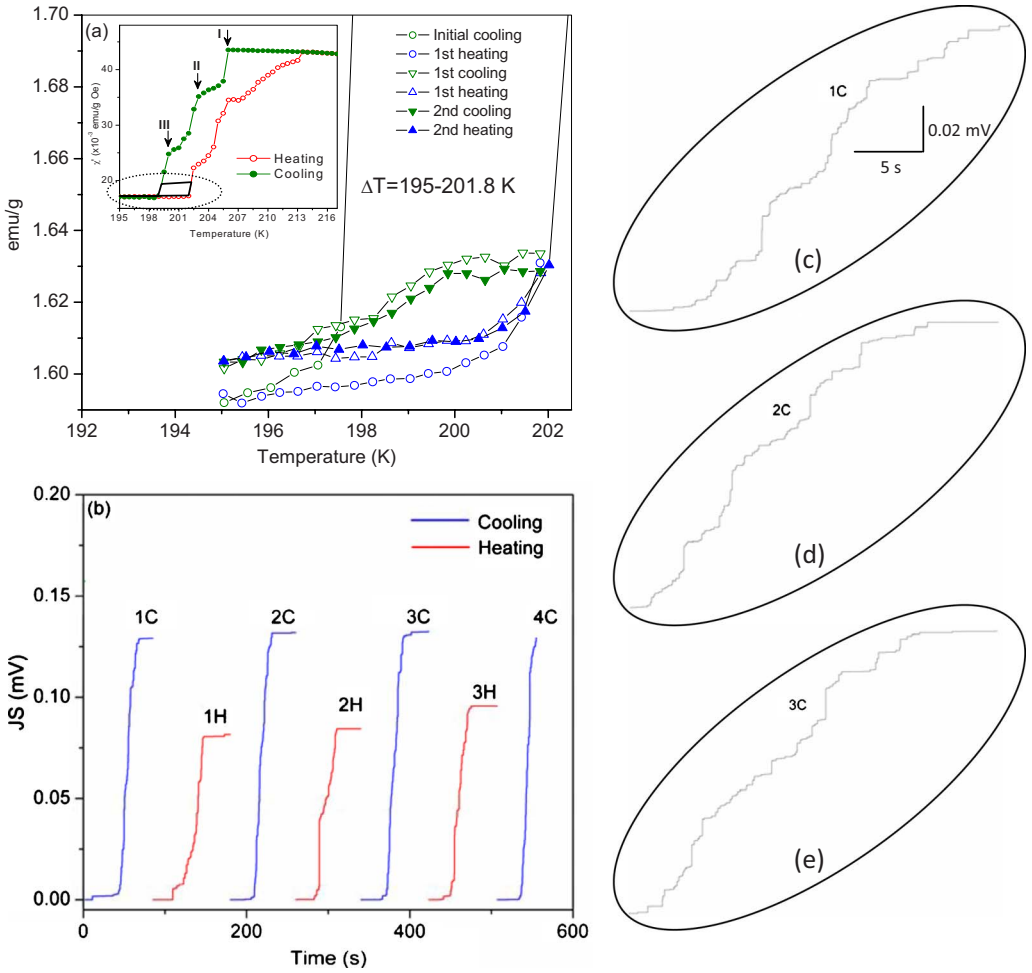

FIG. 13. (Color online) (a) Minor loops of dc magnetization curves at zero-bias field between fully martensitic(III) and martensitic(III-II) regions. (b) Corresponding Jumpsum curves over successive cooling (1C-4C) and heating (1H-3H) cycles. [(c)–(e)] Zoom-in view of three successive Jumsum curves during cooling (1C-3C).

The general expression for the portion of internal energy that is dependent on specific magnetization may be written as

$$E = f(\sigma, T), \tag{1}$$

where E and σ are referred to unit mass.

Basic thermodynamic equations may then be used to derive the general expression for $(\partial E/\partial\sigma)_T$ at constant volume. Note that Eqs. (3)–(10) do not differ from those given by Stoner,[65] and are written here simply for the ease of discussion and derivation of subsequent thermodynamic relationships. From first law of thermodynamics at constant volume, we have

$$dE = TdS + Hd\sigma. \tag{2}$$

Rearranging Eq. (2),

$$dS = \frac{1}{T}dE - \frac{H}{T}d\sigma, \tag{3}$$

$$\Rightarrow \left(\frac{\partial S}{\partial H}\right)_T = \frac{1}{T}\left[\frac{\partial E}{\partial \sigma}\frac{\partial \sigma}{\partial H}\right]_T - \frac{H}{T}\left(\frac{\partial \sigma}{\partial H}\right)_T. \tag{4}$$

Since

$$d(E - TS - H\sigma) = -SdT - \sigma dH. \tag{5}$$

We have from Maxwell relationship using Eq. (5),

$$\left(\frac{\partial S}{\partial H}\right)_T = \left(\frac{\partial \sigma}{\partial T}\right)_H. \tag{6}$$

Substituting for $(\partial S/\partial H)_T$ from Eq. (6) in Eq. (4),

$$\left(\frac{\partial \sigma}{\partial T}\right)_H = \frac{1}{T}\left[\left(\frac{\partial E}{\partial \sigma}\right)_T - H\right]\left(\frac{\partial \sigma}{\partial H}\right)_T. \tag{7}$$

Rearranging Eq. (7) one gets the expression for $(\partial E/\partial\sigma)_T$ in terms of experimentally measurable quantities $(\partial\sigma/\partial T)_H$ and $(\partial\sigma/\partial H)_T$,

$$\left(\frac{\partial E}{\partial \sigma}\right)_T = H + \frac{T(\partial\sigma/\partial T)_H}{(\partial\sigma/\partial H)_T}. \tag{8}$$

Note that Eq. (8) is a general thermodynamic expression for $(\partial E/\partial\sigma)_T$ independent of any particular model of molecular theory of ferromagnetism. By measuring specific magnetization as a function of field and temperature, $\sigma = f(H,T)$, the experimental form of the function $(\partial E/\partial\sigma)_T$ can be determined from Eq. (8). The experimental values of $(\partial\sigma/\partial T)_H$

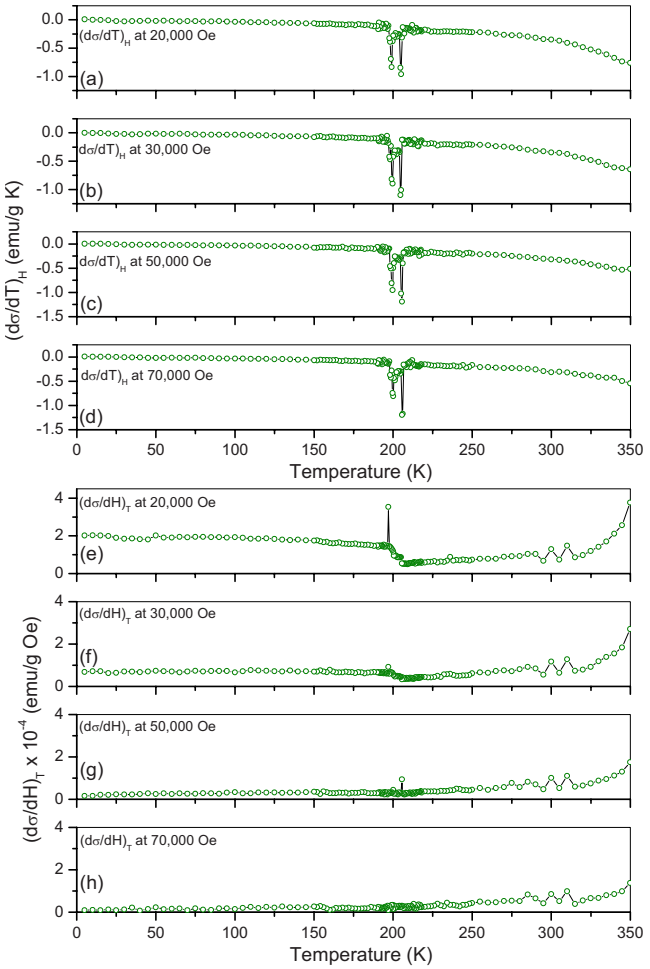

FIG. 14. (Color online) Measured temperature dependence of [(a)–(d)] $(\partial\sigma/\partial T)_H$ and [(e)–(h)] $(\partial\sigma/\partial H)_T$ at different dc bias fields during cooling.

and $(\partial\sigma/\partial H)_T$ at different temperatures at four different bias fields are shown in Figs. 14(a)–14(d) and Figs. 14(e)–14(h), respectively. The magnitudes of these slopes are comparable to those for typical ferromagnets, say, for example, Ni.[66] Next, from a molecular viewpoint, the expression for $(\partial E/\partial\sigma)_T$ in Eq. (8) may be equated to the molecular-field coefficient by the relationship,[65,66]

$$\left(\frac{\partial E}{\partial \sigma}\right)_T = -N\rho\sigma \tag{9}$$

and the σ-dependent portion of internal energy may be written as[65,66]

$$E = -\frac{1}{2}N\rho\sigma^2 = \left(-\frac{1}{\sigma}\right)\left(\frac{\partial E}{\partial \sigma}\right)_T \sigma^2. \tag{10}$$

Knowing $(\partial E/\partial\sigma)_T$ from Eq. (8) (using data from Fig. 14), the temperature dependence of molecular-field coefficient $(N\rho)$ in Eq. (9) can therefore be experimentally determined at different bias fields, as shown in Fig. 15(a) for the present alloy. The inset in Fig. 15(a) shows the zoom-in view of the temperature interval where the successive martensitic transitions occur. Figure 15(b) shows the integral of Fig. 15(a) to

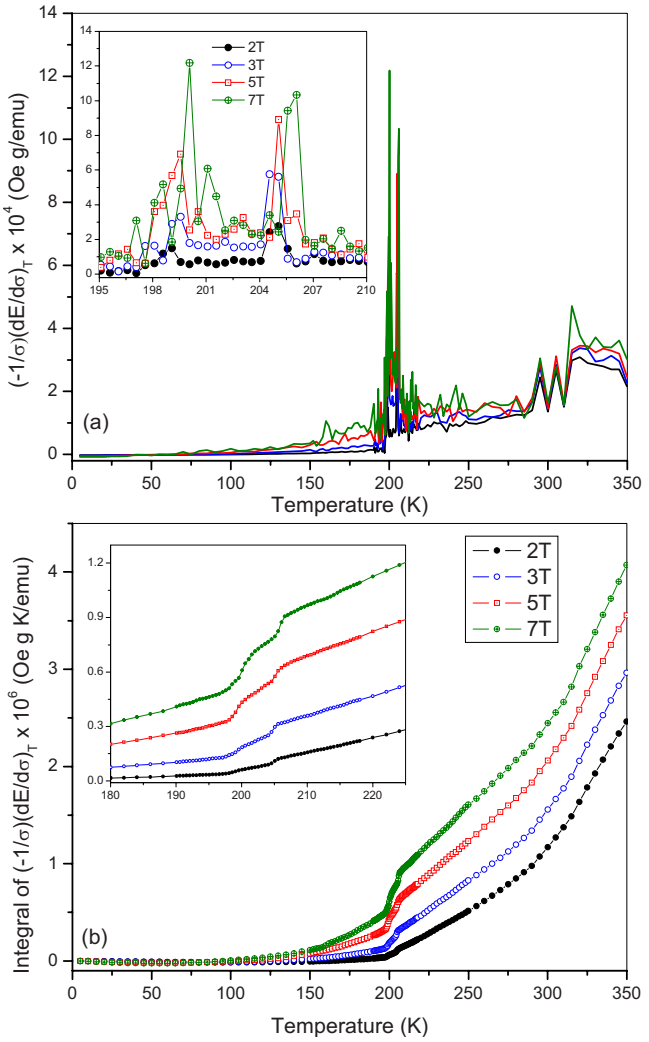

FIG. 15. (Color online) Temperature dependence of molecular-field coefficient $(N\rho)$ at different dc bias fields during cooling. Inset shows the zoom-in view of the temperature interval where martensitic transitions occur. (b) Integral of (a) with inset again highlighting the portion of the temperature interval where martensitic transitions occur. Note that the units of specific magnetization (electromagnetic unit per gram) are equivalent to erg per oersted gram, whereby units for molecular-field coefficient $(N\rho)=(-1/\sigma)(\partial E/\partial\sigma)_H$ are (oersted gram per erg) (erg per gram) (gram per emu) or oersted gram per electromagnetic unit.

better highlight the σ-dependent portion of internal energy as a function of temperature at different applied fields.

1. Relationship between C_H and C_σ

Just as it is more easier to carry out experiments on specific heat at constant pressure C_P than at constant volume C_V, it is easier to carry out measurements of specific heat at constant field C_H than at constant specific magnetization C_σ. However, from a theoretical viewpoint, it is easier to predict specific heat at C_V or C_σ. Therefore, analogous to the well-known relationship between $C_P - C_V = \alpha^2 VT/\beta$ [V is the volume, α is the coefficient of thermal expansion, $(1/V)(\partial V/\partial T)_P$, and β is the coefficient of compressibility

$(-1/V)(\partial V/\partial P)_T$], a relation between $C_H - C_\sigma$ can be derived from the second law of thermodynamics. The following derivation is exact, independent of any model, and differs from an abridged derivation earlier provided by Stoner.[65] To arrive at an expression for $C_H - C_\sigma$, formally we have

$$C_H = (\partial E/\partial T)_H = T(\partial S/\partial T)_H, \tag{11}$$

$$C_\sigma = (\partial E/\partial T)_\sigma = T(\partial S/\partial T)_\sigma. \tag{12}$$

In addition, define the following two quantities:

$$\alpha_H \equiv (\partial \sigma/\partial T)_H \tag{13}$$

and

$$\chi_T \equiv (\partial \sigma/\partial H)_T. \tag{14}$$

In terms of variables (H,T) specific magnetization is

$$d\sigma(H,T) = \left(\frac{\partial \sigma}{\partial H}\right)_T dH + \left(\frac{\partial \sigma}{\partial T}\right)_H dT. \tag{15}$$

Inserting Eqs. (13) and (14) in Eq. (15),

$$d\sigma(H,T) = \chi_T dH + \alpha_H dT. \tag{16}$$

Similarly, we can write for $dS(H,T)$,

$$dS(H,T) = \left(\frac{\partial S}{\partial H}\right)_T dH + \left(\frac{\partial S}{\partial T}\right)_H dT. \tag{17}$$

From Eq. (2), using Maxwell relation, we have

$$\left(\frac{\partial S}{\partial H}\right)_T = \left(\frac{\partial \sigma}{\partial T}\right)_H = \alpha_H. \tag{18}$$

Using Eqs. (11) and (18), Eq. (17) is equal to

$$dS(H,T) = \alpha_H dH + \left(\frac{C_H}{T}\right) dT. \tag{19}$$

Inserting expressions for $d\sigma(H,T)$ and $dS(H,T)$ using Eqs. (16) and (19), respectively, in Eq. (2),

$$dE(H,T) = T\left[\alpha_H dH + \left(\frac{C_H}{T}\right) dT\right] + H[\chi_T dH + \alpha_H dT],$$

$$\Rightarrow dE(H,T) = (T\alpha_H + H\chi_T) dH + (C_H + H\alpha_H) dT. \tag{20}$$

Instead of $E(H,T)$, we can write the expression for $E(\sigma,T)$ by substituting in Eq. (20) the expression for dH from Eq. (16), which gives

$$dE(\sigma,T) = (T\alpha_H + H\chi_T)\left(\frac{1}{\chi_T}\right)(d\sigma - \alpha_H dT) + (C_H + H\alpha_H) dT. \tag{21}$$

Rearranging Eq. (21),

$$dE(\sigma,T) = \left(T\frac{\alpha_H}{\chi_T} + H\right) d\sigma + \left(-\frac{T\alpha_H^2}{\chi_T} + C_H\right) dT. \tag{22}$$

The derivative of Eq. (22) with respect to T at constant σ is C_σ,

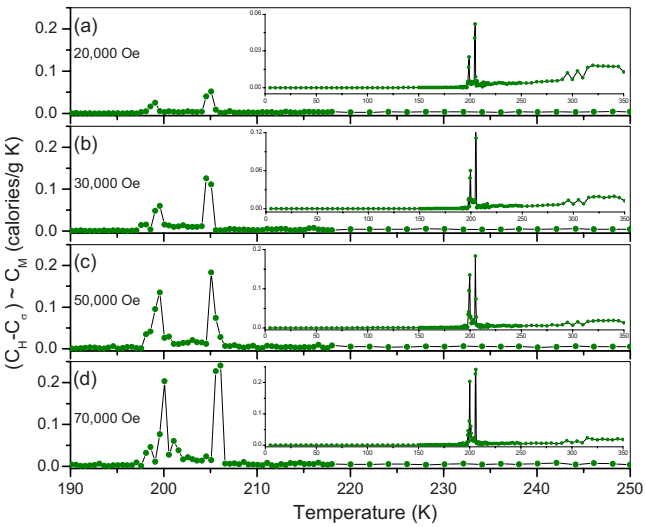

FIG. 16. (Color online) [(a)–(d)] $C_H - C_\sigma$ at different dc bias fields. Insets in (a)–(d) shows the behavior of $C_H - C_\sigma$ over the entire temperature range over which measurements were made. Note that conversion from ergs to calories requires a factor of $\approx 2.39 \times 10^{-8}$.

$$\left(\frac{\partial E}{\partial T}\right)_\sigma = C_\sigma = -T\frac{\alpha_H^2}{\chi_T} + C_H \tag{23}$$

or

$$C_H - C_\sigma = T\frac{\alpha_H^2}{\chi_T}. \tag{24}$$

Notice the comparative role of terms α_H and χ_T in the expression for $C_H - C_\sigma$ in Eq. (24) versus those in expression for $C_P - C_V = \alpha^2 VT/\beta$. Substituting in Eq. (24) the expressions for α_H and χ_T from Eqs. (13) and (14), respectively,

$$C_H - C_\sigma = \frac{T(\partial \sigma/\partial T)_H^2}{(\partial \sigma/\partial H)_T}. \tag{25}$$

The right-hand side of Eq. (25) is in terms of measurable quantities shown earlier in Fig. 14. The behavior of $C_H - C_\sigma$ as a function of temperature at different fields is shown in Fig. 16; the equality between $C_H - C_\sigma$ and magnetic specific heat C_M is shown in the next section. The insets in Fig. 16 show the behavior over the entire temperature range. From the general relation $(\frac{\partial z}{\partial x})_y(\frac{\partial x}{\partial y})_z(\frac{\partial y}{\partial z})_x = -1$ for a function $z(x,y)$, one obtains

$$\left(\frac{\partial \sigma}{\partial T}\right)_H \left(\frac{\partial H}{\partial \sigma}\right)_T \left(\frac{\partial T}{\partial H}\right)_\sigma = -1 \tag{26}$$

or

$$-\frac{(\partial H/\partial T)_\sigma}{(\partial H/\partial \sigma)_T} = \left(\frac{\partial \sigma}{\partial T}\right)_H. \tag{27}$$

Using Eq. (27), Eq. (24) becomes

$$C_H - C_\sigma = \frac{T(\partial\sigma/\partial T)_H^2}{(\partial\sigma/\partial H)_T} = \frac{T(\partial\sigma/\partial T)_H}{(\partial\sigma/\partial H)_T}\left[-\frac{(\partial H/\partial T)_\sigma}{(\partial H/\partial\sigma)_T}\right] = -T\left(\frac{\partial H}{\partial T}\right)_\sigma\left(\frac{\partial\sigma}{\partial T}\right)_H. \quad (28)$$

Using Eqs. (8) and (27), Eq. (28) can be written as

$$C_H - C_\sigma = \left\{\left(\frac{\partial E}{\partial\sigma}\right)_T - H\right\}\left(\frac{\partial\sigma}{\partial T}\right)_H. \quad (29)$$

2. Estimation of magnetic specific heat C_M from $C_H - C_\sigma$

The excess specific heat of a ferromagnet (at a given field, including the zero field for the case of spontaneous magnetization) differs from the specific heat of a similar material lacking in ferromagnetism. This excess magnetic specific heat C_M is given by

$$C_M = \left(\frac{\partial E}{\partial T}\right)_H = \left(\frac{\partial E}{\partial\sigma}\right)\left(\frac{\partial\sigma}{\partial T}\right) = \frac{1}{2}\left(\frac{1}{\partial}\frac{\partial E}{\partial\sigma}\right)\left(\frac{\partial\sigma^2}{\partial T}\right). \quad (30)$$

But $(-1/\sigma)(\partial E/\partial\sigma)_T$ is the molecular-field coefficient $N\rho$. Therefore,

$$C_M = -\frac{1}{2}N\rho\left(\frac{\partial\sigma^2}{\partial T}\right). \quad (31)$$

And, in particular, for the case of spontaneous magnetization at zero field,

$$C_{M,H=0} = \left(\frac{\partial E}{\partial\sigma_o}\right)\left(\frac{\partial\sigma_o}{\partial T}\right) = \frac{1}{2}\left(\frac{1}{\sigma_o}\frac{\partial E}{\partial\sigma_o}\right)\left(\frac{\partial\sigma_o^2}{\partial T}\right) = -\frac{1}{2}(\rho N_{H=0})\left(\frac{\partial\sigma_o^2}{\partial T}\right). \quad (32)$$

It was the ratio $(C_{M,H=0}/\rho N_{H=0})$ in Eq. (32) that was earlier plotted in Fig. 10(b).

From Eqs. (9) and (29),

$$C_H - C_\sigma = \left\{\left(\frac{\partial E}{\partial\sigma}\right)_T - H\right\}\left(\frac{\partial\sigma}{\partial T}\right)_H = (-N\rho\sigma - H)\left(\frac{\partial\sigma}{\partial T}\right)_H = -N\rho\sigma\left(1 + \frac{H}{N\rho\sigma}\right)\left(\frac{\partial\sigma}{\partial T}\right)_H. \quad (33)$$

Since $N\rho\sigma \gg H$,

$$C_H - C_\sigma \cong N\rho\sigma\left(\frac{\partial\sigma}{\partial T}\right)_H = -\frac{1}{2}N\rho\left(\frac{\partial\sigma^2}{\partial T}\right) = C_M. \quad (34)$$

In other words, $(C_H - C_\sigma)$ is essentially a measure of C_M and the error in this approximation is negligible ($\sim$1 part per million) even in fields as high as several teslas. Thus, knowing the values of $(C_H - C_\sigma)$ from experimental data, C_M can be estimated or *vice versa*, as indicated by the approximate equality in Fig. 16.

Note that at temperatures away from phase transitions (in particular, away from martensitic transitions), in the single phase regime where all the above equations hold, the values of magnetic specific heat ($\sim$millicalories per gram kelvin) are comparable to what one would find for a typical ferromagnet, such as, for example, Ni.[66,67] *The derived values of* C_M at phase transitions are to be used cautiously given that the above equations are valid for a single phase only and at constant volume. In particular, the values of C_M at martensitic phase transformations are not valid given the large self-strains involved in martensitic phase transformations.

3. Form of the function $(\partial E/\partial\sigma)_T$

Finally, by substituting $-N\rho\sigma$ for $(\partial E/\partial\sigma)_T$, Eq. (7) can be written as

$$\left(\frac{\partial\sigma}{\partial T}\right)_H = -\left(\frac{H + N\rho\sigma}{T}\right)\left(\frac{\partial\sigma}{\partial H}\right)_T. \quad (35)$$

Seek solutions of the form

$$\sigma(H,T) = f(\eta), \quad (36)$$

where

$$\eta \equiv \frac{H + N^*(T)\rho\sigma}{T}. \quad (37)$$

To determine the relation between N and $N^*(T)$, we have

$$\left(\frac{\partial\sigma}{\partial T}\right)_H = \left(\frac{\partial f}{\partial\eta}\right)\frac{\partial}{\partial T}\left[\frac{H + N^*(T)\rho\sigma}{T}\right]_H \quad (38)$$

$$= f'\left\{-T^{-2}(H + N^*\rho\sigma) + T^{-1}\left[N^{*\prime}\rho\sigma + N^*\rho\left(\frac{\partial\sigma}{\partial T}\right)_H\right]\right\}. \quad (39)$$

Therefore,

$$\left(\frac{\partial\sigma}{\partial T}\right)_H = \frac{f'}{T}\left\{-\eta + N^*\rho\sigma\left(\frac{N^{*\prime}}{N^*} + \frac{(\partial\sigma/\partial T)_H}{\sigma}\right)\right\}. \quad (40)$$

Rearranging Eq. (40),

$$\left(\frac{T}{f'} - N^*\rho\right)\left(\frac{\partial\sigma}{\partial T}\right)_H = -\eta + (\rho\sigma)N^{*\prime}, \quad (41)$$

$$\Rightarrow\left(\frac{\partial\sigma}{\partial T}\right)_H = \frac{-\eta + (\rho\sigma)N^{*\prime}}{\left(\frac{T}{f'} - N^*\rho\right)}. \quad (42)$$

Also,

$$\left(\frac{\partial\sigma}{\partial H}\right)_T = \left(\frac{\partial f}{\partial\eta}\right)\frac{\partial}{\partial H}\left[\frac{H + N^*(T)\rho\sigma}{T}\right]_T \quad (43)$$

$$= \frac{f'}{T}\left[1 + N^*\rho\left(\frac{\partial\sigma}{\partial H}\right)_T\right] \quad (44)$$

or

$$\left(\frac{T}{f'} - N^*\rho\right)\left(\frac{\partial\sigma}{\partial H}\right)_T = 1. \quad (45)$$

Rearranging Eq. (45),

$$\frac{1}{\left(\frac{T}{f'} - N^*\rho\right)} = \left(\frac{\partial\sigma}{\partial H}\right)_T. \tag{46}$$

Using Eq. (46), Eq. (42) is equal to

$$\left(\frac{\partial\sigma}{\partial T}\right)_H = \left(\frac{\partial\sigma}{\partial H}\right)_T [-\eta + (\rho\sigma)N^{*\prime}]. \tag{47}$$

Substituting for η from Eq. (37),

$$= -\left[\left(\frac{H + N^*(T)\rho\sigma}{T}\right) - (N^{*\prime}\rho\sigma)\right]\left(\frac{\partial\sigma}{\partial H}\right)_T, \tag{48}$$

$$\Rightarrow \left(\frac{\partial\sigma}{\partial T}\right)_H = -\left\{\left[\frac{H + (N^* - N^{*\prime})\rho\sigma}{T}\right]\right\}\left(\frac{\partial\sigma}{\partial H}\right)_T, \tag{49}$$

where

$$\left[\frac{H + (N^* - N^{*\prime})\rho\sigma}{T}\right] = \left(\frac{H + N\rho\sigma}{T}\right). \tag{50}$$

Hence,

$$N = N^* - \frac{\partial N^*}{\partial T}T. \tag{51}$$

It is again *reiterated* that the above thermodynamic equations are valid for a given single phase, under the condition that magnetic hysteretic effects are absent and the observed change in volume for any given phase are relatively small. Based on these caveats, experimental derivations of various thermodynamic properties were performed only at sufficiently high fields ($\geq$20 kOe) to eliminate possible magnetic hysteretic effects, thereby ensuring that the measured specific magnetization is equal to the intrinsic specific magnetization. In the two phase regions when only a small change in volume occurs from one phase to another, the experimental data may still be valid by viewing the thermodynamic quantity of interest as being proportional to the volume fraction of the two phases.

IV. CONCLUSIONS

We conclude the existence of phase transitions from steps in the intrinsic thermodynamic property, namely, spontaneous magnetization. Spontaneous magnetization—magnetization within a single magnetic domain of the crystal at zero magnetic field—and its variation with temperature is the fundamental thermodynamic quantity of interest in characterizing any given magnetic phase. Steps in spontaneous magnetization versus temperature are the representation of magnetic phase transitions in the truest thermodynamic sense. The observation of multiple phase transitions in Ni-Mn-Ga Heusler alloy is directly corroborated with direct optical observations as well as jumps in spontaneous atomic moments at the critical points.

Differences in temperatures where the steps in spontaneous magnetization versus, for example, ac susceptibility, are easily explained. The difference arises because derivation of spontaneous magnetization is an extrapolation of data to zero field and shall differ from directly measured data such as dc magnetization or ac susceptibility.

Observation of three different martensitic phase transitions in the same volume eliminates effects as arising from composition gradients. One might consider the hypothesis of some sort of surface transition. This possibility is eliminated because such a region would have only a small magnetization change associated with it and is not compatible with the overall observed data, including a large signal in magnetic transition spectra, large macroscopic shears observable in movies, steps in spontaneous magnetization, etc. The dynamics of micromagnetic reconfiguration take an infinite number of pathways resembling a devil's staircase while the system repeatedly achieves the same final state.

The observed field dependence of molecular-field coefficient at any given field is linked to the field susceptibility of the observed transitions. From general thermodynamics considerations, the magnetic specific heat is shown to be equal to the difference in heat capacities at constant field and magnetization. As a result, its values can be experimentally deduced. Finally, the form of the function for intrinsic specific magnetization is formally derived.

ACKNOWLEDGMENTS

This work was supported by the National Science Foundation, Grant Nos. DMR-0706074 and DMR-0305242, and this support is gratefully acknowledged. The authors acknowledge useful discussions with Antoni Planes at Department d'Estructura i Constituents de la Matèria, Universitat de Barcelona, Barcelona, Catalonia, Spain, and for providing us with the single crystal of Heusler alloy. H.D.C. acknowledges Manfred Wuttig at the University of Maryland for discussions related to possible applicability of Devil's staircase to the current problem.

*Corresponding author; hchopra@buffalo.edu

[1] B. Matthias and A. von Hippel, Phys. Rev. **73**, 1378 (1948).
[2] P. W. Forsbergh, Phys. Rev. **76**, 1187 (1949).
[3] A. von Hippel, Rev. Mod. Phys. **22**, 221 (1950).
[4] W. L. Roth, J. Appl. Phys. **31**, 2000 (1960).
[5] J. N. Armstrong, M. R. Sullivan, and H. D. Chopra, Phys. Rev. B **80**, 104429 (2009).
[6] Z. S. Basinski and J. W. Christian, Acta Metall. **2**, 148 (1954).
[7] A. Saxena, S. R. Shenody, A. R. Bishop, Y. Wu, and T. Lookman, Phase Transitions **67**, 481 (1998).
[8] H. D. Chopra, C. Bailly, and M. Wuttig, Acta Mater. **44**, 747 (1996).
[9] H. D. Chopra, A. L. Roytburd, and M. Wuttig, Metall. Mater. Trans. A **27**, 1695 (1996).
[10] Z. P. Li, Sci. China, Ser. A: Math., Phys. Astron. **47**, 165 (2004).
[11] K. Ullakko, J. K. Huang, C. Kantner, R. C. O. Handley, and V. V. Kokorin, Appl. Phys. Lett. **69**, 1966 (1996).
[12] V. A. Chernenko, E. Cesari, V. V. Kokorin, and I. N. Vitenko,

Scr. Metall. Mater. **33**, 1239 (1995).
[13] A. N. Vasil'ev, A. D. Bozhko, V. V. Khovailo, I. E. Dikshtein, V. G. Shavrov, V. D. Buchelnikov, M. Matsumoto, S. Suzuki, T. Takagi, and J. Tani, Phys. Rev. B **59**, 1113 (1999).
[14] H. D. Chopra, C. Ji, and V. V. Kokorin, Phys. Rev. B **61**, R14913 (2000).
[15] V. V. Kokorin and M. Wuttig, J. Magn. Magn. Mater. **234**, 25 (2001).
[16] M. De Graef, Y. Kishi, Y. Zhu, and M. Wuttig, International Conference on Martensitic Transformations, 2002, Part 2 [J. Phys. IV **112** 993 (2003)].
[17] V. A. Chernenko, V. A. L'Vov, P. Mullner, G. Kostorz and T. Takagi, Phys. Rev. B **69**, 134410 (2004).
[18] M. R. Sullivan, D. A. Ateya, S. J. Pirotta, A. A. Shah, G. H. Wu, and H. D. Chopra, J. Appl. Phys. **95**, 6951 (2004).
[19] M. R. Sullivan and H. D. Chopra, Phys. Rev. B **70**, 094427 (2004).
[20] M. R. Sullivan, A. A. Shah and H. D. Chopra, Phys. Rev. B **70**, 094428 (2004).
[21] M. R. Sullivan, S. J. Pirotta, V. A. Chernenko, G. H. Wu, G. Balasubramanium, S. Z. Hua, and H. D. Chopra, Int. J. Appl. Electromagn. Mech. **22**, 11 (2005).
[22] G. Li and Y. Liu, Appl. Phys. Lett. **88**, 232504 (2006).
[23] B. L. Ahuja, B. K. Sharma, S. Mathur, N. L. Heda, M. Itou, A. Andrejczuk, Y. Sakurai, A. Chakrabarti, S. Banik, A. M. Awasthi and S. R. Barman, Phys. Rev. B **75**, 134403 (2007).
[24] S. Aksoy, T. Krenke, M. Acet, E. F. Wassermann, X. Moya, L. Manosa and A. Planes, Appl. Phys. Lett. **91**, 241916 (2007).
[25] T. Krenke, E. Duman, M. Acet, E. F. Wassermann, X. Moya, L. Manosa, A. Planes, E. Suard and B. Ouladdiaf, Phys. Rev. B **75**, 104414 (2007).
[26] X. Moya, L. Manosa, A. Planes, S. Aksoy, M. Acet, E. F. Wassermann and T. Krenke, Phys. Rev. B **75**, 184412 (2007).
[27] S. Banik, R. Rawat, P. K. Mukhopadhyay, B. L. Ahuja, A. Chakrabarti, P. L. Paulose, S. Singh, A. K. Singh, D. Pandey and S. R. Barman, Phys. Rev. B **77**, 224417 (2008).
[28] J. N. Armstrong, M. R. Sullivan, M. Le Romancer, V. A. Chernenko and H. D. Chopra, J. Appl. Phys. **103**, 023905 (2008).
[29] D. Niklasch, J. Dadda, H. J. Maier, and I. Karaman, J. Mater. Sci. **43**, 6890 (2008).
[30] B. Ludwig, C. Strothkaemper, U. Klemradt, X. Moya, L. Manosa, E. Vives and A. Planes, Appl. Phys. Lett. **94**, 121901 (2009).
[31] A. Planes, L. Manosa and M. Acet, J. Phys.: Condens. Matter **21**, 233201 (2009).
[32] Y. M. Jin, Acta Mater. **57**, 2488 (2009).
[33] Y. M. Jin, Appl. Phys. Lett. **94**, 062508 (2009).
[34] P. J. Webster, K. R. A. Ziebeck, S. L. Town, and M. S. Peak, Philos. Mag. B **49**, 295 (1984).
[35] A. Zheludev, S. M. Shapiro, P. Wochner, A. Schwartz, M. Wall, and L. E. Tanner, Phys. Rev. B **51**, 11310 (1995).
[36] J. Worgull, E. Petti, and J. Trivisonno, Phys. Rev. B **54**, 15695 (1996).
[37] A. Zheludev, S. M. Shapiro, P. Wochner, and L. E. Tanner, Phys. Rev. B **54**, 15045 (1996).
[38] U. Stuhr, P. Vorderwisch, V. V. Kokorin, and P. A. Lindgård, Phys. Rev. B **56**, 14360 (1997).
[39] L. Mañosa, A. Gonzàlez-Comas, E. Obradó, A. Planes, V. A. Chernenko, V. V. Kokorin, and E. Cesari, Phys. Rev. B **55**, 11068 (1997).
[40] A. Planes, E. Obradó, A. Gonzàlez-Comas, and L. Mañosa, Phys. Rev. Lett. **79**, 3926 (1997).
[41] A. Gonzàlez-Comas, E. Obradó, L. Mañosa, A. Planes, V. A. Chernenko, B. J. Hattink, and A. Labarta, Phys. Rev. B **60**, 7085 (1999).
[42] L. Mañosa, A. Planes, J. Zarestky, T. Lograsso, D. L. Schlagel, and C. Stassis, Phys. Rev. B **64**, 024305 (2001).
[43] J. von Boehm and P. Bak, Phys. Rev. Lett. **42**, 122 (1979).
[44] W. Kinzel and K. Binder, Phys. Rev. B **24**, 2701 (1981).
[45] P. Bak, Rep. Prog. Phys. **45**, 587 (1982).
[46] P. Bak and R. Bruinsma, Phys. Rev. Lett. **49**, 249 (1982).
[47] R. A. Cowley, D. A. Jehan, D. F. McMorrow, and G. J. McIntyre, Phys. Rev. Lett. **66**, 1521 (1991).
[48] S. E. Burkov, Phys. Rev. B **44**, 2850 (1991).
[49] R. Bruinsma and J. Prost, J. Phys. II **4**, 1209 (1994).
[50] X. Y. Wang and P. L. Taylor, Phys. Rev. Lett. **76**, 640 (1996).
[51] K. Ohwada, Y. Fujii, N. Takesue, M. Isobe, Y. Ueda, H. Nakao, Y. Wakabayashi, Y. Murakami, K. Ito, Y. Amemiya, H. Fujihisa, K. Aoki, T. Shobu, Y. Noda, and N. Ikeda, Phys. Rev. Lett. **87**, 086402 (2001).
[52] M. Yakes, V. Yeh, M. Hupalo, and M. C. Tringides, Phys. Rev. B **69**, 224103 (2004).
[53] W. Steurer, Acta Crystallogr. Sect. A: Found. Crystallogr. **61**, 28 (2005).
[54] T. Yamauchi, H. Ueda, J.-I. Yamaura, and Y. Ueda, Phys. Rev. B **75**, 014437 (2007).
[55] H. D. Chopra and M. R. Sullivan, Rev. Sci. Instrum. **76**, 013910 (2005).
[56] H. Barkhausen, Phys. Z. **20**, 401 (1919).
[57] M. R. Sullivan, D. A. Ateya, S. Pirotta, A. A. Shah, G. H. Wu and H. D. Chopra, *Materials and Devices for Smart Systems*, edited by Y. Furuya, E. Quandt, Q. Zhang, K. Inoue, and M. Shahinpoor, Vol. 785 (Materials Research Society, Boston, MA, 2004), pp. 457–467.
[58] L. J. Swartzendruber, G. E. Hicho, H. D. Chopra, S. D. Leigh, G. Adam, and E. Tsory, J. Appl. Phys. **81**, 4263 (1997).
[59] H. D. Chopra, G. E. Hicho, and L. J. Swartzendruber, Mater. Eval. **59**, 1215 (2001).
[60] See supplementary material at http://link.aps.org/supplemental/10.1103/PhysRevB.81.174405 for a movie showing three successive martensite transformations in the same volume of the sample as it is being cooled. See description of Fig. 3 in the text for details. The second movie shows the repeated annihilation and reformation of ferroelastic domains during heating and cooling cycles between 195 and 201.8 K, corresponding to the transition between martensite(III) and martensite(III-II) phase regions. The second movie corresponds to *JS* curves shown in Fig. 13.
[61] T. A. Sandenaw and J. F. Andrew, J. Nucl. Mater. **173**, 59 (1990).
[62] B. Ludwig, C. Strothkaemper, U. Klemradt, X. Moya, L. Manosa, E. Vives, and A. Planes, Phys. Rev. B **80**, 144102 (2009).
[63] P. Weiss and R. Forrer, Ann. Phys. (Paris) **5**, 153 (1926).
[64] D. J. Oliver and W. Sucksmith, Proc. R. Soc. London, Ser. A **219**, 1 (1953).
[65] E. C. Stoner, Philos. Mag. **19**, 565 (1935).
[66] E. C. Stoner, Philos. Trans. R. Soc. London **235**, 165 (1936).
[67] K. E. Grew, Proc. R. Soc. London, Ser. A **145**, 509 (1934).